Chapter 5

Astronomical spectra

Observational astronomical spectra are not only a direct recording of the observed emitted flux of a distant source as a function of wavelength, F_λ, but also of the absorption, scattering, and emission that modifies F_λ due to material along the light path to the observer.

The utility of astronomical spectra is that the observed flux can be transformed into physical conditions at the emission source, in the proximity of the emission source, and/or of material intervening to the source. There are limits, however. Often, the physical properties deduced from spectra can be reduced no further than to integrated quantities. And, as we will discuss, many implicit assumptions are lurking in the analysis (for example, assuming isotropic emission from the source, and/or assuming the optical depth is uniform across the beam cross section).

In this chapter, we discuss these assumption in the context of absorption from material intervening to an emitting source. We discuss the scenario in which the material fully occults the source and in which the material only partially occults the source (i.e., partial covering). We then show how the optical depth of a single absorption feature can be written as the product of the column density of the absorbing atomic species column density and the atomic absorption cross section, $\alpha(\lambda)$. Thermal and/or dynamic motions of the atomic absorbers result in a substantial spread in the distribution of photon wavelengths absorbed due to the Doppler shifts. We briefly describe the thermal broadening in absorption features via the probability distribution of atomic absorbers removing photons at "offset" wavelengths. The dynamical broadening is incorporated into the optical depth using the total absorption cross section, $\sigma(\lambda)$. We then discuss magnitudes and photometric systems and conclude by addressing atmospheric attenuation of the observed flux.

5.1 Absorption in astronomical spectra

In § 4.1.4, we derived F_λ for an unocculted, unresolved spherical source of radius R_s at a distance D from the observer under highly simplifying assumptions (these assumption were restated in § 4.1.4). Here, we formulate the flux integral more generally by (1) relaxing the assumptions applied to the emitting source, and (2) applying the solution of the 1–D equation of transfer for sources fully occulted and partially occulted by an intervening absorption cloud. Finally, we discuss modifications to the observed astronomical spectrum for ground based observations.

5.1.1 Relaxing isotropy of the source

Consider a non–isotropic emitting source with specific intensity distribution $\mathcal{I}_\lambda(R, \phi, \theta)$ such that the emitted intensity varies with the (ϕ, θ) locations on the source surface. In the most general case, the source surface may not be spherical, i.e., $R = R(\phi, \theta)$. Applying the treatments presented in § 4.1.3, the observed flux of an unocculted, unresolved source is

$$F_\lambda = \frac{R_s^2}{D^2} \int_0^{2\pi} \int_0^{\pi/2} \mathcal{I}_\lambda(R, \phi, \theta) \cos\theta \sin\theta \, d\theta \, d\phi, \tag{5.1}$$

where it has been assumed that the observer is located a distance D from the source on the $+z$ axis, i.e., in the direction $\theta = 0$ (see Figure 4.2). Recall that the polar angle ranges from $0 \leq \theta \leq \pi/2$ for integration over the "near–side" hemisphere of the source. By relaxing isotropy, the non–constant $\mathcal{I}_\lambda$ cannot be factored out of the integral.

5.1.2 Intervening absorption

The schematic of the geometric configuration of an absorbing cloud intervening to the emitting source is presented in Figure 5.1. Assume the source is unresolved. The line of sight to the observer for a single beam element is shown as originating from an area element located at arbitrary azimuthal and polar angular positions ϕ and θ with respect to the geometric center of the source. From the observer's point of view, this beam element passes through the absorbing cloud at polar coordinate $R \sin\theta, \phi$ on the cloud face (in the plane of the sky).

To incorporate the absorption into the calculation of the observed flux, we simply invoke the solution of the transfer equation for pure absorption (Eq. 4.49) and insert it into Eq. 5.1. We have

$$F_\lambda = \frac{R_s^2}{D^2} \int_0^{2\pi} \int_0^{\pi/2} \mathcal{I}_\lambda(R, \phi, \theta) \exp\{-\tau_\lambda(\phi, \theta)\} \cos\theta \sin\theta \, d\theta \, d\phi. \tag{5.2}$$

Note that the total optical depth through the cloud, $\tau_\lambda(\phi, \theta)$, must pair with each $\mathcal{I}_\lambda(R, \phi, \theta)$ and is therefore a function of the azimuthal and polar angular

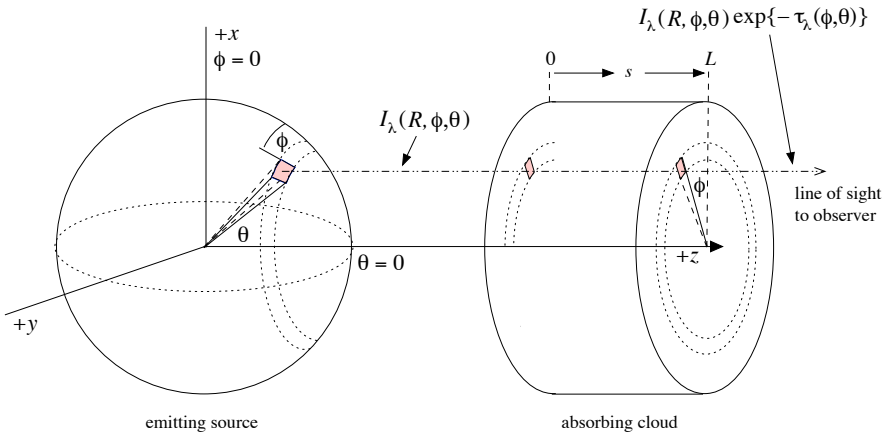

Figure 5.1: Non–isotropic specific intensity $\mathcal{I}_\lambda(R,\phi,\theta)$ is emitted from an area element on the non–spherical surface $R(\phi,\theta)$ at azimuthal and polar angular positions ϕ and θ, respectively, with respect to the source center. The beam passes through an absorbing cloud intervening to the observer at a location in the cloud corresponding to the ϕ and θ angular positions where the beam originated on the source. If the absorption coefficient is not constant throughout the intervening cloud, then the total optical depth attentuating this particular $\mathcal{I}_\lambda(R,\phi,\theta)$ is $\tau_\lambda(\phi,\theta)$; that is, the total optical depth corresponds to the $R\sin\theta,\phi$ location $\mathcal{I}_\lambda$ probes the cloud, which depends upon the ϕ,θ location from which $\mathcal{I}_\lambda$ was emitted from the source. The distance from the source to the observer is D along the $+z$ axis. The distance of the intervening cloud from the source and from the observer is arbitrary.

positions ϕ and θ, the point of origin of the specific intensity on the source surface. This allows for non–uniform attenuation of different lines of sight through the absorbing cloud. Invoking Eq. 4.37, the total optical depth as a function of ϕ,θ is

$$\tau_\lambda(\phi,\theta) = \int_0^{L(\phi,\theta)} \chi_\lambda(s,\phi,\theta)\,ds, \tag{5.3}$$

for a path length $L(\phi,\theta)$ throught the cloud, where we allow that the cloud may have non–uniform thickness.

Thus, a full treatment of Eq. 5.2 to obtain the observed attenuated flux in each wavelength interval, $\lambda \rightarrow \lambda + d\lambda$, requires an integral over the surface of the source for which the optical depth through the intervening cloud associated with each $\mathcal{I}_\lambda(R,\phi,\theta)$ element depends upon the ϕ,θ point of origin on the source surface. The integral can only be evaluated if the optical depth corresponding to each $\mathcal{I}_\lambda(R,\phi,\theta)$ is known; in practice, the mapping is an intractable problem–when the source is unresolved, there is no observational data that can provide the functional form of $\chi_\lambda(s,\phi,\theta)$ within the cloud nor of the path length $L(\phi,\theta)$ through the cloud.

The only way to evaluate Eq. 5.2 is to assume $\mathcal{I}_\lambda(R,\phi,\theta)$ and $\tau(\phi,\theta)$ are independent of both ϕ and θ so that they can be factored out of the integral. The common practice is to assume the source radiates isotropically, so that $\mathcal{I}_\lambda(R,\phi,\theta) = \mathcal{I}_\lambda(R)$, and that $R = R_s$ is constant (a spherical source). An

average cloud optical depth is also assumed, i.e., $\bar{\tau}_\lambda = \bar{\chi}_\lambda \langle L \rangle$, where $\bar{\chi}_\lambda$ and $\langle L \rangle$ are the mean extinction coefficient and mean total path length through the cloud, respectively. None of these quantities can be known *a priori*.

The above assumptions may appear obvious and even somewhat trivial; however, it is worth explicitely formulating the problem of calculating the absorption by an intervening cloud for an unresolved astronomical source. The point here is to emphasize that virtually all published extragalactic work necessarily rests upon these simplifying assumptions. Applying the assumptions and evaluating Eq. 5.2, the observed flux is

$$F_\lambda = \frac{R_s^2}{D^2} \pi \mathcal{I}_\lambda(R_s) \exp\left\{-\bar{\tau}_\lambda\right\} = \frac{R_s^2}{D^2} \mathcal{F}_\lambda \exp\left\{-\bar{\tau}_\lambda\right\}, \tag{5.4}$$

where $\mathcal{F}_\lambda$ is the astrophysical flux of the source (Eq. 4.17).

5.1.3 Partial covering

The above treatment was based upon the assumption that the radiating source is fully occulted by the intervening absorbing cloud. This condition may not always hold true. Even if a source is unresolved from the perspective of the observer, it is possible that the geometric configuration of the source and absorber is such that the source is not fully occulted. This is known as partial covering. When partial covering is present, some beams carrying specific intensity $\mathcal{I}_\lambda$ interact with the absorbing cloud (are occulted) and are modified as dictated by the transfer equation, whereas the remainder of the beams propagate to the observer without modification (are not occulted).

A simplistic example of partial covering is schematically illustrated in Figures 5.2*a* (face on view) and 5.2*b* (side view). In this scenario, the observed solid angle of the intervening cloud is smaller than the observed solid angle of the source.

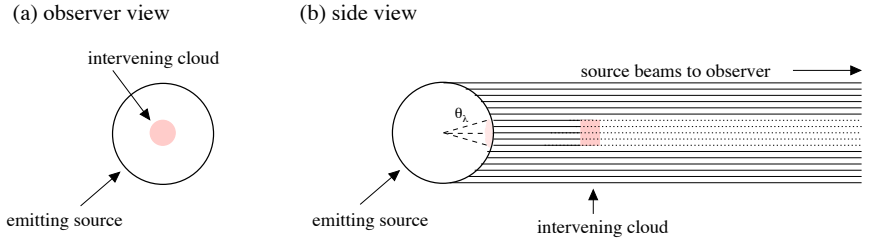

Figure 5.2: A schematic of partial covering scenarios. Solid lines from the isotropic source are specific intensity beams that are unobstructed by the intervening absorber, whereas dotted lines are beams for which some level of absorption has occurred. A highly idealized case in which the observed solid angle of the absorbing cloud (shaded) is smaller than the observed solid angle of the source. In this scenario, the intervening cloud occults a area on the source (lightly shaded) defined by a cone with angle θ_λ. (*a*) Face–on view. (*b*) Side view.

For heuristic purposes, we assume (1) from the observers perspective, the intervening cloud is directly aligned with the center of a spherical source and

that the projected cross section of the intervening cloud is circular, (2) the emitted specific intensity is isotropic, so that $\mathcal{I}_\lambda(R_s, \phi, \theta) = \mathcal{I}_\lambda(R_s)$, and (3) the optical depth through the intervening cloud is uniform and constant, so that it is independent of the location and path of the beam sight line through the cloud, and therefore independent of the location from which the beam originated on the surface of the source, i.e., $\tau_\lambda(\theta, \phi) = \tau_\lambda$. As shown in Figure 5.2*b*, the solid angle of the region of the source that is occulted subtends an angle θ_λ, where the subscript λ generalizes the possibility that the projected cross section can vary with wavelength.

From the observer point of view, the beams originating from the surface of the source within the range of polar angles $0 \leq \theta \leq \theta_\lambda$ will be occulted by the cloud, and those in the annulus $\theta_\lambda \leq \theta \leq \pi/2$ will by unocculted. From the fundamental theorem of calculus, Eq. 5.2 can be expressed as the sum

$$F_\lambda = F_\lambda^u + F_\lambda^t, \tag{5.5}$$

where F_λ^u is the observed flux from the unocculted sight lines and F_λ^t is the observed transmitted flux, i.e., the flux comprising photons from the sight lines passing through the intervening absorption cloud that were not absorbed. The transmitted flux is,

$$\begin{aligned} F_\lambda^t &= \frac{R_s^2}{D^2} \int_0^{2\pi} \int_0^{\theta_\lambda} \mathcal{I}_\lambda(R_s) \exp\{-\tau_\lambda\} \cos\theta \sin\theta \, d\theta \, d\phi \\ &= \sin^2\theta_\lambda \, \frac{R_s^2}{D^2} \mathcal{F}_\lambda \exp\{-\tau_\lambda\}, \end{aligned} \tag{5.6}$$

and the unocculted flux is

$$\begin{aligned} F_\lambda^u &= \frac{R_s^2}{D^2} \int_0^{2\pi} \int_{\theta_\lambda}^{\pi/2} \mathcal{I}_\lambda(R_s) \cos\theta \sin\theta \, d\theta \, d\phi \\ &= \left[1 - \sin^2\theta_\lambda\right] \, \frac{R_s^2}{D^2} \mathcal{F}_\lambda. \end{aligned} \tag{5.7}$$

Substituting F_λ^u and F_λ^t into Eq. 5.5 yields

$$F_\lambda = \left[1 - \sin^2\theta_\lambda\right] \frac{R_s^2}{D^2} \mathcal{F}_\lambda + \sin^2\theta_\lambda \frac{R_s^2}{D^2} \mathcal{F}_\lambda \exp\{-\tau_\lambda\}. \tag{5.8}$$

Note that if the geometeric factor is $\sin^2\theta_\lambda = 0$, then the observed flux is unattenuated, and if $\sin^2\theta_\lambda = 1$, then the observed flux is for a fully occulted source. Common practice is to define this geometric factor as a wavelength dependent covering fraction, $f_c(\lambda)$. Clearly, the functional form of the covering fraction depends upon the assumed geometric configuration; for the above idealized scenario $f_c(\lambda) = \sin^2\theta_\lambda$. Defining $F_\lambda^0 = (R_s^2/D^2)\mathcal{F}_\lambda$ as the observed flux of an unocculted source yields the functional form commonly quoted in the scientific literature,

$$R_\lambda = \frac{F_\lambda}{F_\lambda^0} = [1 - f_c(\lambda)] + f_c(\lambda) \exp\{-\tau_\lambda\}, \tag{5.9}$$

where the first term on the right hand side represents flux from unocculted sight lines and the second term represents the flux transmitted through the cloud.

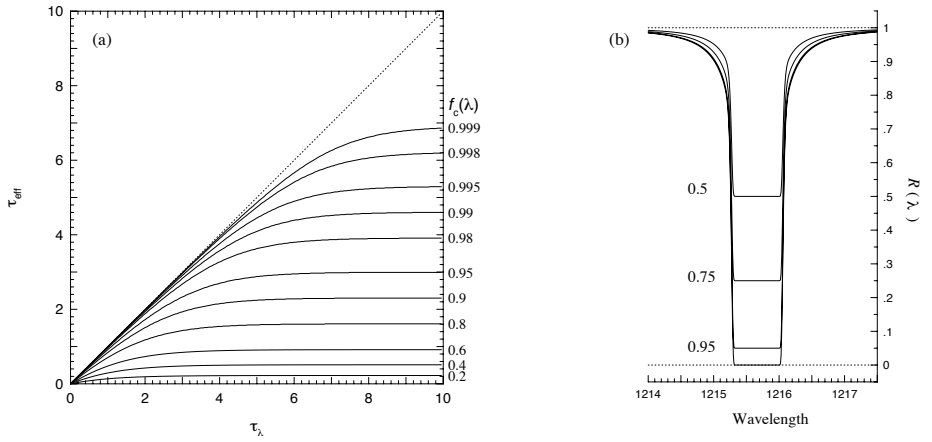

Figure 5.3: (*a*) The effective, or measured, optical depth $\tau_{\rm eff}$, obtained by inverting the flux ratio R_λ versus the mean optical depth in the cloud, τ_λ for various covering fractions, $f_c(\lambda)$. (*b*) An example "black–bottomed" absorption profile with $\tau_\lambda \gg 10$ in the profile center for $f_c(\lambda) = 0.50, 0.75$, 0.95, and 1.00.

We define the effective optical depth, $\tau_{\rm eff}$, as that which is measured directly from the flux ratio in a spectrum, $R_\lambda = \exp\{-\tau_{\rm eff}\}$. The relationship between a selected range of $\tau_{\rm eff}$, τ_λ, and $f_c(\lambda)$, as given by Eq. 5.9, is illustrated in Figure 5.3*a*. Note that even if the τ_λ of a partially occulting cloud is very large, a non–negligible amount of flux can be transmitted to the observer for non–zero $f_c(\lambda)$.

Consider the scenario for which the flux transmitted through the absorbing cloud, F_λ^t, is vanishingly small; for example when $\tau_\lambda \gg 10$. If the cloud fully occulted the source, zero flux would be recorded in the center of the absorption profile (such a profile is often referred to as being "black bottomed"). However, in the case of partial covering, when $F_\lambda^t = f_c(\lambda)\exp\{-\tau_\lambda\} \simeq 0$, Eq. 5.9 yields $R_\lambda = 1 - f_c(\lambda)$. In Figure 5.3*b*, an example absorption profile from a cloud with $\tau_\lambda \gg 10$ in the absorption profile center is illustrated for $f_c(\lambda) = 0.50, 0.75$, 0.95, and 1.00 (full occultation). Note, that for a lone absorption profile that would have a "black–bottomed" core in the case of unity covering factor, the covering fraction can be read directly from R_λ and $\tau_{\rm eff}$ can be easily computed; however, τ_λ cannot be determined.

5.2 Column Density

An astronomical spectrum is the recording $I_\lambda/I_\lambda^0 = \exp\{-\tau_\lambda\}$. As such, the optical depth at each wavelength is the only quantity from which the physical conditions of the absorbing gas can be deduced. Upon substitute of Eqs. 4.25

and 4.35 into Eq. 4.37, the optical depth is expressed

$$\tau_\lambda = \int_0^L \Big[\sum_{ijk} n_{ijk}(s)\, \alpha_{ijk}(\lambda) \Big] ds, \tag{5.10}$$

where n_{ijk} is the number density of atoms of species k that are in one of all possible ionization stages, j, and excitation states, i, $\alpha_{ijk}(\lambda)$ is the atomic absorption cross section at wavelength λ, $n_e(s)$ is the density of free electrons, and where we have ignored scattering.

Thus, at first glance, it would seem impossible to deduce the physical state of the absorbing gas from the measured optical depth since there is degeneracy between the various possible combinations of all the $n_{ijk}(s)\, \alpha_{ijk}(\lambda)$; it is a problem of hundreds of unknowns combined to give a single known. Fortunately, as illustrated in Figure 4.7*a*, the absorption cross sections for bound–bound transitions are highly peaked over an extremely narrow wavelength range, on the order of $\Delta\lambda \simeq 10^{-4}$ Å. Thus, once an observed absorption profile is "identified", meaning that it is known to be due to a given electron transition from a given species in a given ionization and excitation state, then Eq. 5.10 collapses to a single term for the relevant wavelength range,

$$\tau_\lambda = \int_0^L n(s)\, \alpha(\lambda)\, ds, \tag{5.11}$$

where $n(s)$ is the number density of the relevant absorber as a function of the line of sight location, $\alpha(\lambda)$ is the cross section for the relevant interaction, and where we assume there is no scattering contribution to the attenuation over the wavelength range of the feature. Since $\alpha(\lambda)$ is based upon atomic physics, it is independent of line of sight position and can be factored out of the integral,

$$\tau_\lambda = \alpha(\lambda) \int_0^L n(s)\, ds \tag{5.12}$$

Defining the column density, N, as the number density of absorbers integrated along the line of sight path length,

$$N = \int_0^L n(s)\, ds, \tag{5.13}$$

which has unit [atoms cm^{-2}], we obtain the simplified result that the optical depth is the product of the column density and the absorption cross section [cm^2],

$$\tau_\lambda = N\alpha(\lambda). \tag{5.14}$$

Eq. 5.14 is extremely powerful; the measured optical depth (albeit over a narrow wavelength range) is now reduced to a single number, the column density of the absorbing atomic species giving rise to the absorption profile. Thus, because the functional form of $\alpha(\lambda)$ is known, N can be directly determined from the observed spectrum according to

$$F_\lambda = F_\lambda^0 \exp\left\{-N\alpha(\lambda)\right\}. \tag{5.15}$$

This is the most commonly applied form of the solution to the transfer equation under the conditions of a background emitting source observed through an absorbing cloud (no internal emission and unity covering fraction).

5.3 Doppler broadening

Observed absorption profiles are significantly broader than the natural widths of the atomic absorption cross sections. The additional broadening is due to the thermal (and/or turbulent) motions of the atomic absorbers.

5.3.1 Observed shifts

Consider a single absorbing atom in motion within an absorbing cloud. The line of sight component of the motion of this atom with respect to the source results in a wavelength shift in the absorption cross section, $\alpha(\lambda)$, in the observer reference frame.

Let the velocity vector of a single atom be $\mathbf{v} = v_x\hat{\mathbf{i}}+v_y\hat{\mathbf{j}}+v_z\hat{\mathbf{k}}$ with magnitude $v^2 = v_x^2 + v_y^2 + v_z^2$, which is known as the particle speed. Assume that both the absorbing cloud and the observer are at rest with respect to the source. The line of sight samples the absorbing cloud in a single spatial direction; thus, the observed line of sight velocity component is the dot product of the line of sight propagation direction of the beam, $\hat{\mathbf{s}}$, and the velocity vector of the atom,

$$v_o = -\mathbf{v}\cdot\hat{\mathbf{s}}, \tag{5.16}$$

where the negative sign provides the convention $v_o > 0$ for components toward the source and away from the observer and $v_o < 0$ for components away from the source and toward the observer. A scematic of the geometric realtionship between $\mathbf{v}$, $\hat{\mathbf{s}}$, and v_o is illustrated in Figures 5.4*a* and 5.4*b*. Note that $\hat{\mathbf{s}}$ is the vector direction from source to observer.

As illustrated in Figure 4.7, the absorption cross section for bound–bound transitions are extremely narrow, with $\Delta\lambda \simeq 10^{-4}$ Å. Due to the Doppler shift, absorbing atoms will "see" all source photon wavelengths shifted by the amount $\Delta\lambda/\lambda = -v_o/c = (\mathbf{v}\cdot\hat{\mathbf{s}})/c$ (consider the source velocity from the atom's point of view). If the wavelength at the narrow peak of the absorption cross section is λ_r in the rest–frame of the atom, then in the frame of the absorbing cloud and the observer, the observed peak will have wavelength

$$\lambda_o = \lambda_r\left(1 + \frac{v_o}{c}\right). \tag{5.17}$$

As illustrated in Figure 5.4*c*, for $v_o > 0$ (velocity component toward source), the observed wavelength of the peak, λ_o, is shifted redward relative to λ_r. And, as illustrated in Figure 5.4*d*, for $v_o < 0$ (velocity component toward observer), λ_o is shifted blueward relative to λ_r. An extremely tiny v_o will result in a significant shift of the absorption cross section peak relative to its width. If $\lambda_r \sim 1000$ Å, typical of atomic bound–bound transitions, a v_o on the order of 0.03 km sec^{-1} results in an observed shift of the cross section equal to its full width.

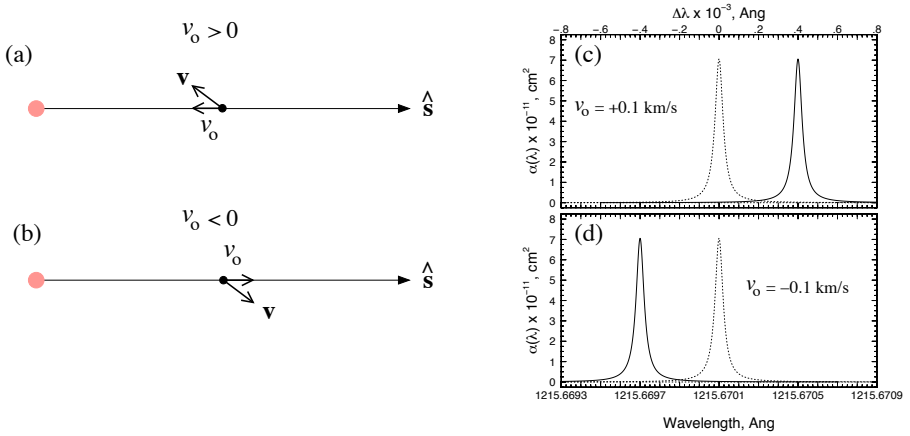

Figure 5.4: (*a*) Schematic of the line of sight velocity component, v_o, of an atom with velocity vector $\mathbf{v}$ for which the component is positive and away from the observer (in the negative $\hat{\mathbf{s}}$ direction). (*b*) Same as panel *a*, but for a negative v_o due to motion toward the observer. (*c*) Illustration of the wavelength shift in the absorption cross sections for neutral hydrogen in the ground state calculated from Eq. 5.17. The dashed curve is the rest–frame cross section, peaking at $\lambda_r = 1215.6701$ Å. The solid curve is the observed shift corresponding to the schematic in panel *a*, for $v_o = +0.1$ km sec^{-1}. (*d*) Same as for panel *c*, but for the schematic in panel *b* for $v_o = -0.1$ km sec^{-1}. For the example velocity, which is quite small, the observed shift of $\Delta\lambda = 0.0004$ Å is roughly four times the full width of the cross section.

5.3.2 Broadening in an isothermal medium

Since each atom shifts the absorption cross section in proportion to its line of sight velocity according to Eq. 5.17, it follows that there will be a distribution of observed velocity shifts in the absorber cross sections and this distribution will depend upon the fractional number of absorbers in a given velocity interval, dv. This "Doppler broadening" modifies the optical depth as a function of observed wavelength.

It is always possible that the line of sight velocity of a given absorbing atom depends upon its location in the cloud (such as in a galactic wind or accretion structure). In such cases, the density of absorbing atoms at a given velocity may also dependent on location in the cloud. In simpler cases, it may be reasonable to assume that the absorber velocities are not dependent upon location, but only upon the temperature of the gas. Regardless of the complexity of the scenario, the distribution of wavelength shifts of the absorption cross sections will depend upon a model of the gas kinematics.

Here, we illustrate the influence of a simple distribution of velocities on the redistribution of absorption with observed wavelength. We assume an isothermal cloud in which the density and velocity of the absorbing atoms is independent of location. This scenario commonly applied. For a non–relativistic isothermal gas, the distribution of particle velocities is the well–known Maxwellian distribution.

For purpose of illustration, assume $\hat{\mathbf{s}} = \hat{\mathbf{k}}$, that line of sight vector is parallel to the $+z$ direction, the direction to the observer. Consider an isothermal gas

cloud comprising particles of atomic species k having mass m. If $n_k(v_z)\,dv_z$ is the number density of particles of species k in the velocity interval $v_z \to v_z + dv_z$, and n_k is the number density of all particles of species k, then the fraction within the interval $v_z \to v_z + dv_z$ is written $f(v_z)\,dv_z = [n_k(v_z)/n_k]\,dv_z$, which has the functional form

$$f(v_z)\,dv_z = \left(\frac{m}{2\pi kT}\right)^{1/2} \exp\left\{-\frac{mv_z^2}{2kT}\right\}\,dv_z, \tag{5.18}$$

where kT is the product of the Boltzmann constant k [erg K^{-1}] and the temperature, T [K]. The normalization is

$$\int_0^\infty f(v_z)\,dv_z = 1. \tag{5.19}$$

Since v_z was arbitrarily (and conveniently) chosen to be the velocity along the line of sight to the observer, we have $v_o = v_z$. Thus, Eq. 15.1 describes the observed line of sight component of the velocity distribution, $f(v_o)\,dv_o$.

The distribution of particle speeds, $f(v)\,dv_x dv_y dv_z = [n_k(v)/n_k]\,dv_x dv_y dv_z$ in the interval $v_x \to v_x + dv_x$, $v_y \to v_y + dv_y$, and $v_z \to v_z + dv_z$, is given by

$$f(v)\,dv_x dv_y dv_z = f(v_x)f(v_y)f(v_z)\,dv_x dv_y dv_z \tag{5.20}$$

where $v^2 = v_x^2 + v_y^2 + v_z^2$. The cartesian velocity element $dv_x dv_y dv_z$ containing the velocity interval $v_x \to v_x + dv_x$, $v_y \to v_y + dv_y$, and $v_z \to v_z + dv_z$ is replaced in Eq. 15.3 by the spherical element $4\pi v^2 dv$, which can be visualized as a shell of thickness $v \to v + dv$. The distribution of particle speeds is then

$$f(v)\,dv = \left(\frac{m}{2\pi kT}\right)^{3/2} \exp\left\{-\frac{mv^2}{2kT}\right\} 4\pi v^2 dv, \tag{5.21}$$

with

$$\int_0^\infty f(v)\,dv = 1. \tag{5.22}$$

Eqs. 15.1 and 15.5 are the well–known Maxwellian velocity and speed distribution functions, respectively.

The observed line of sight velocity distributions (v_o, Eq. 15.1) are illustrated in Figure 15.2*a* for hydrogen at three temperatures, illustrating that the distribution dispersion increases and the amplitude decreases with increasing T. In Figure 15.2*b*, the dependence with species atomic mass is shown for the common elements hydrogen, carbon, magnesium, and iron at $T = 50,000$ [K]. Note that the distribution dispersion decreases and the amplitude increases with increasing particle mass. The Maxwellian speed distributions (Eq. 15.5) are shown in Figures 15.2*c* and 15.2*d*, respectively for hydrogen at three temperatures and for hydrogen, carbon, magnesium, and iron at $T = 50,000$ [K].

For the Maxwellian speed distribution, the most probable speed, v_0, the average speed, $\langle v \rangle$, and the RMS speed, $v_{\rm RMS}$, are

$$v_0 = \left(\frac{2kT}{m}\right)^{1/2} \qquad \langle v \rangle = \left(\frac{8}{\pi}\frac{kT}{m}\right)^{1/2} \qquad v_{\rm RMS} = \left(\frac{3kT}{m}\right)^{1/2}. \tag{5.23}$$

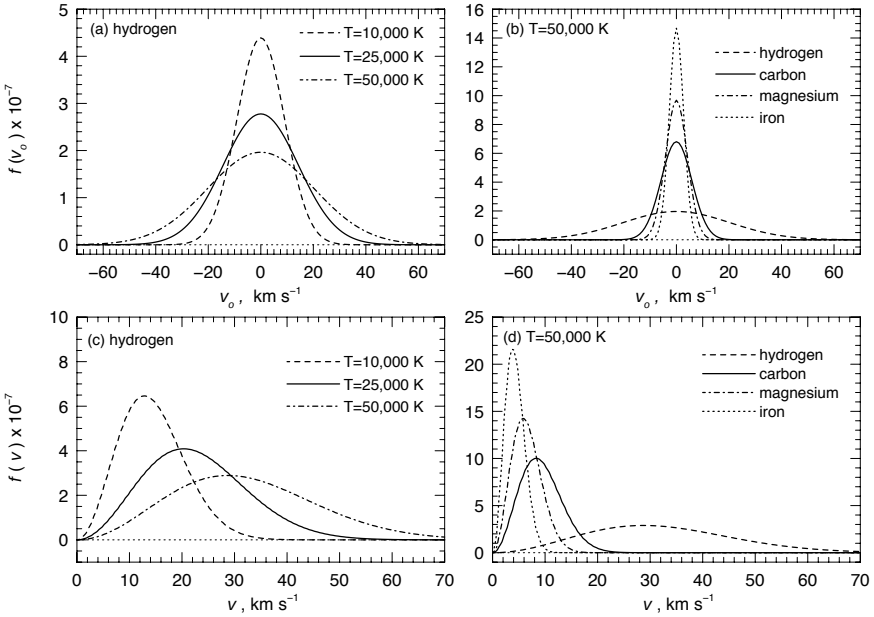

Figure 5.5: The Maxwellian distribution of particle speeds and one–dimensional velocity components. (*a*) The distribution of the observed line of sight component of velocity, v_o, for hydrogen at $T = 10,000$, $25,000$, and $50,000$ [K]. (*b*) The distribution of v_o for hydrogen, carbon, magnesium, and iron at $T = 50,000$ K. (*c*) The distribution of particle speeds, v, for hydrogen at $T = 10,000$, $25,000$, and $50,000$ [K]. (*d*) The distribution of v for hydrogen, carbon, magnesium, and iron at $T = 50,000$ [K].

For a given T, note that heavier particles have smaller v_0, $\langle v \rangle$, and $v_{\rm RMS}$. In terms of the most probable speed, v_0, Eq. 15.1 can be written

$$f(v_o)\,dv_o = \frac{1}{\sqrt{\pi}v_0}\exp\left\{-\left(\frac{v_o}{v_0}\right)^2\right\}dv_o, \tag{5.24}$$

where v_0 can now be interpreted as $\sqrt{2}\,\sigma$, where σ is the standard deviation of a unit area Guassian distribution. Note that it is assumed that there is no systemic line of sight velocity to the ensemble of atoms, i.e., $v_{sys} = 0$. If this assumption were relaxed, then all appearances of v_o in Eq. 5.24 would be replaced by the velocity difference $\Delta v = v_o - v_{sys}$.

Via the Doppler shift, $\Delta\lambda/\lambda = v/c$, the observed distribution of the wavelengths of the absorption cross section peaks, λ_r, will obey the functional form of Eq. 5.24, but with $\sqrt{2}\,\sigma$ written

$$\Delta\lambda_{\rm D} = \frac{v_0}{c}\lambda_r = \frac{\lambda_r}{c}\left(\frac{2kT}{m}\right)^{1/2}, \tag{5.25}$$

which is known as the characteristic Doppler width. Employing the principle of the Doppler shift, with $\Delta\lambda = \lambda - \lambda_r$, and substituting Eq. 5.25 into Eq. 5.24,

we obtain the observed wavelength shift distribution,

$$f(\Delta\lambda)\,d\lambda = \frac{1}{\sqrt{\pi}\Delta\lambda_{\rm D}} \exp\left\{ -\left(\frac{\Delta\lambda}{\Delta\lambda_{\rm D}}\right)^2 \right\} d\lambda. \tag{5.26}$$

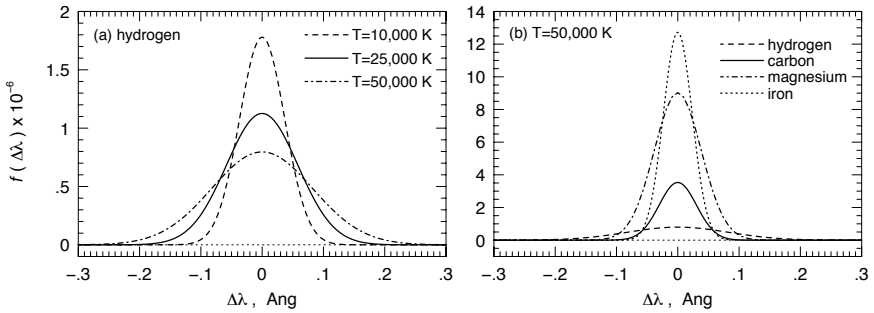

Figure 5.6: The Doppler shift distribution due to the Maxwellian distribution of the observed line of sight velocity distribution of absorbers. (*a*) The distribution of $\Delta\lambda$ for the ground state neutral hydrogen transition Lyα λ1215 at $T = 10,000$, $25,000$, and $50,000$ [K]. (*b*) The distribution of $\Delta\lambda$ at $T = 50,000$ [K] for the selected transitions: neutral hydrogen (HI λ1215), triple ionized carbon (CIV λ1548), single ionized magnesium (MgII λ2796), and single ionized iron (FeII λ2600).

Selected examples of observed line of sight wavelength distributions for the peak wavelengths of the absorber cross sections are illustrated in Figure 5.6 as a function of $\Delta\lambda = \lambda - \lambda_r$. Because $\Delta\lambda_{\rm D}$ is proportional to λ_r, each distribution function is specific to a given absorption transition. In Figure 5.6*a*, the observed distribution of $\Delta\lambda$ is shown for the Lyα λ1215 neutral hydrogen transition at $T = 10,000$, $25,000$, and $50,000$ [K]. In Figure 5.6*b*, the observed distribution is shown for four transitions commonly found in astronomical spectra (see figure caption).

Note that the amplitude of the observed velocity distribution (Eq. 5.24) scales with $(m/T)^{1/2}$ and the width scales as the inverse, $(T/m)^{1/2}$. However, the amplitude of the observed wavelength distribution (Eq. 5.26) scales with $\lambda_r^{-1}(m/T)^{1/2}$ and the width scales as the inverse $\lambda_r(T/m)^{1/2}$. Figures 15.2*b* and 5.6*b* clearly illustrate these differences.

The full widths of the thermal distributions (Figure 5.6) are a factor of few $\times$ 10^3 broader than the widths of the atomic absorption cross sections (Figure 4.7). Therefore, the thermal conditions of the gas can have a dominating influence on the resulting wavelength dependence of the optical depth, τ_λ, and therefore the "shape" (depth and width) of absorption lines.

5.4 The total absorption cross section

Due to thermal broadening, the expression for the optical depth as given by Eqs. 5.11 and 5.14,

$$\tau_\lambda = \int_0^L n(s)\,\alpha(\lambda)\,ds = N\alpha(\lambda), \tag{5.27}$$

must be modified to account for the distribution of wavelength shifts in the narrow and highly peaked absorption cross section, $\alpha(\lambda)$. The total absorption cross section for a given transition is obtained via convolution of the atomic absorption cross section with the probability distribution of observed wavelengh shifts,

$$\sigma(\lambda) = \alpha(\lambda) \otimes f(\Delta\lambda). \tag{5.28}$$

Note that $f(\Delta\lambda)$, as written in Eq. 5.26, is a true probability function and provides the probability that the atomic absorption cross section will be shifted an amount $\Delta\lambda$. The probability is, in simple terms, given by the fraction of atomic absorbers that have line of sight velocity v_o such that they see the incoming radiation Doppler shifted by $\Delta\lambda$. The total absorption cross section, $\sigma(\lambda)$, is actually a function of several quantities: (1) the mass of the absorbing atomic species, m, (2) the gas temperature, T, and (3) the atomic constants (see § 16.1.2) that dictate the shape and amplitude of $\alpha(\lambda)$.

The convolution to obtain $\sigma(\lambda)$ as a function of wavelength requires evaluating a series of integrals, each centered on a given λ

$$\sigma(\lambda) = \int_0^\infty \alpha(\lambda')f(\lambda' - \lambda)\,d\lambda', \tag{5.29}$$

over the variable λ', which samples the wavelength dependence of the distribution function, $f(\Delta\lambda)$. Visualize Eq. 5.29 as the process of centering the peak of $f(\Delta\lambda)$ at a given λ, integrating over λ', and then repeating at each λ. As long as there is no net systemic motion to the ensemble of absorbing particles, the resulting $\sigma(\lambda)$ will peak at λ_r, the peak of the atomic absorption cross section. Eq. 5.29 simply weights $\alpha(\lambda')$ by $f(\lambda' - \lambda)\,d\lambda'$ at each interval $\lambda' \rightarrow \lambda' + d\lambda'$.

Returning to the expression of the optical depth as formulated in Eq 5.11, with inclusion of the isothermal broadening we have

$$\tau_\lambda = \int_0^L n(s)\,\sigma(\lambda)\,ds = N\sigma(\lambda), \tag{5.30}$$

where N is the column density of the absorbing atomic species for the targeted transition in the spectrum. The observed flux across the profile of a single feature in an astronomical spectrum can now be written in terms of the total absorption coefficient

$$F_\lambda = F_\lambda^0 \exp\left\{-N\sigma(\lambda)\right\}. \tag{5.31}$$

From Eq. 5.31, both the column density of the absorbing atomic species and the Doppler width (and therefore gas temperature) can be directly deduced from the observed flux in an astronomical spectrum. As we shall illustrate in subsequent

discussion (see § 16.3), there can be degeneracy between N and T in certain regimes of N.

Although the absorption cross sections for bound–free (ionization) absorption features, as illustrated in Figure 4.7*b*, can extend over a larger wavelength range, it is still possible to employ Eq. 5.31 to obtain the column density of atoms undergoing ionization. In fact, since the absorption cross section for bound–free absorption varies smoothly over a very broad wavelength range, the convolution given by Eq. 5.29 is effectively unnecessary. The widths of the $f(\Delta\lambda)$ are on the order of 0.1 Å (see Figure 5.6), whereas the bound–free cross sections vary smoothly over ~ 1000 Å (see Figure 4.7).

5.5 Recap of assumptions

Ultimately, the functional form of the integrand of Eq. 5.30 is based upon a model of the absorbing gas cloud. The Maxwellian distribution of observed line of sight absorbing atom velocities is one such model; in fact, it is a very simplistic model based upon assumptions designed to simplify the radiative transfer through an absorbing medium. An isothermal model cloud must be assumed if $\sigma(\lambda)$ is to be factored out of the optical depth integral over s, the line of sight path. As such, the application of Eq. 5.31 requires the assumption of no spatial variation in the gas temperature along the line of sight.

In principle, the integral for the optical depth (Eq. 5.30) can be very complex. For any absorbing cloud model in which the total absorption cross section is expressed as a function of s, it will be impossible to factor $\sigma(\lambda)$ out of the integral and therefore neatly write the optical depth in terms of column density, i.e., $\tau_\lambda \neq N\sigma(\lambda)$. If systematic kinematics, bulk flows, and/or turbulent motions are to be included in the optical depth model of the absorbing cloud, then the distribution function, $f(\Delta\lambda)$, may be difficult to formulate, difficult to convolve with the atomic absorption cross section (Eq. 5.29), difficult to integrate over the path length (Eq. 5.30), or possibly all three difficulties apply. Moreover, a model might be constructed in which the density of absorbing atoms, $n(s)$, is a function of the gas kinematics.

In any event, Eq. 5.31 is the most commonly utilized expression relating the observed flux to the optical depth for the case of a purely absorbing intervening gas cloud. To emphasize that the derivation of Eq. 5.31 has been based upon several assumptions, we review them here:

- an unresolved, spherical isotropic emittng source of radius, $\mathcal{I}_\lambda(R_s)$, where otherwise $\mathcal{I}_\lambda(R, \phi, \theta)$ with $R = R(\phi, \theta)$
- an absorbing cloud intervening to the source that fully occults the source
- neglibile emission and neglibile scattering within the intervening absorbing cloud

- a constant optical depth, $\tau_\lambda = \bar{\chi}_\lambda \langle L \rangle$, across the beam cross section (so that the absorption is independent of the point of origin of a beam element emitted from the source)

- atomic absoption cross sections that depend only upon the atomic physics, i.e., are independent of the local physical environment [under certain conditions $\alpha(\lambda)$ can be modified, such as in the presence of magnetic fields or high gas pressure]

- an isothermal absorbing gas cloud, so that the total absorption cross section, $\sigma(\lambda)$, is independent of line of sight location through the cloud [allowing $\sigma(\lambda)$ to be factored out of optical depth integral (Eq. 5.30)]

As each of these assumptions is relaxed, either the solution to the radiative transfer and/or the expression for the optical depth become progressively more complex. Eq. 5.31 is employed for most all applications in the astronomical literature.

In practice, greater complexity is applied when the structure of a global absorbing phenomenon is being studied or the kinematics of such a structure is being studied. Examples of applications for which the models of the radiative transfer and/or optical depth are more complex include intergalactic gas structures undergoing cosmological expansion (e.g., Gunn & Peterson, 1965), rotating galactic halos with density gradients (e.g., Weisheit, 1978), infalling clouds into galactic halos and rotating galaxy disk kinematics (e.g., Lanzetta & Bowen, 1992) and outflowing winds associated with the background source itself (e.g., Vilkovoiskij & Irwin, 2001).

The reader is also refered to the books on stellar atmospheres by Mihalas (1978) and by Gray (1992). These authors, especially Mihalas, develop formalism of the optical depth for absorption models that incorporate systematic gas dynamics.

5.6 Spectrophotometry and Magnitudes

In certain applications, it may be of interest to measure the observed flux, F_λ, summed over a desired wavelength range. This converts the energy collected per unit area per unit time per unit wavelength to energy collected per unit area per unit time. The flux per unit wavelength, F_λ is sometimes referred to as the flux density, whereas the quantity $F(\lambda) = \lambda F_\lambda$ is referred to as the flux (in this text, this distinction of nomenclature is applied only when the context of discussion requires it; the subscript always implies flux density). The flux over a selected wavelength range is written

$$F = \int_{\lambda_-}^{\lambda_+} \lambda F_\lambda \, d\lambda, = \int_{\lambda_-}^{\lambda_+} F(\lambda) \, d\lambda, \tag{5.32}$$

where λ_- and λ_+ are the lower and upper limits of the wavelength range.

Alternatively, the flux density and flux can be measured or converted to frequency units, where $F(\nu) = \nu F_\nu$, where the frequency flux density, F_ν, has units of [erg s^{-1} cm^{-2} Hz^{-1}]. The relationship between F_ν and F_λ derive from energy conservation and the relationship $c = \nu\lambda$. We have

$$F_\lambda d\lambda = F_\nu d\nu, \qquad F_\lambda = \frac{c}{\lambda^2} F_\nu \,. \tag{5.33}$$

In the application of Eq. 5.33, to preserve units between F_λ and F_ν, the factor $d\nu/d\lambda = c/\lambda^2$ is computed in "mixed" units. Writing $d\nu/d\lambda = (c/\lambda)/\lambda$, we compute c/λ in cgs units with the final λ in [angströms].

In imaging, it is common that the observed flux is measured using a fixed filtered band pass. It is also common practice that the filter is a member of a predetermined suite of filters comprising a photometric system (see below). These photometric systems are calibrated using the magnitude system. Magnitudes are unitless numbers on an inverted logarithmic scale that are based upon flux ratios. The zero points are defined by the fluxes of standard objects accounting for the filter band–pass response of the filters.

In cases where spectroscopic data are in hand but the magnitude of the source is desired in a certain band pass, one can perform spectrophotometry. If the response function of the filter with band pass y is $R_y(\lambda)$ over the wavelength range λ_{y^-} to λ_{y^+}, then the measured band pass flux (modulated by the filter band pass) is

$$F_y = \int_{\lambda_{y^-}}^{\lambda_{y^+}} R_y(\lambda)\, F_\lambda \, d\lambda \,. \tag{5.34}$$

The response functions are the probability of transmission at each wavelength and obey

$$\int_{\lambda_{y^-}}^{\lambda_{y^+}} R_y(\lambda)\, d\lambda = 1, \tag{5.35}$$

where the integration is take over a broad enough wavelength range such that the filter response vanishes, i.e., $R_y(\lambda) = 0$ for $\lambda = \lambda_{y^-}$ and $\lambda = \lambda_{y^+}$.

5.6.1 Apparent magnitude

The flux density measured on the magnitude scale is defined by

$$m_\lambda = -2.5 \log F_\lambda \qquad m_\nu = -2.5 \log F_\nu \tag{5.36}$$

As such, magnitudes provide an alternative scale with which flux densities can be quoted. It is not uncommon to see the flux densities of stars and other sources presented in m_λ or m_ν.

The band–pass apparent magnitude is defined using the ratio of the band–pass flux (Eq, 5.34) of the object to that of a standard source. In a band pass y,

$$m_y = -2.5 \log \left\{ \frac{F_y}{F_y^s} \right\} \tag{5.37}$$

where F_y is the band pass y flux of the object and F_y^s is band pass y flux of the standard source. Note that if the object band pass flux equals the source band pass flux, i.e., $F_y = F_y^s$, then $m_y = 0$. Thus, the standard source provides the zero point of the apparent magnitude scale. Also, note that m_y decreases as the ratio F_y/F_y^s increases. Objects with $F_y > F_y^s$ have $m_y < 0$ and those with $F_y > F_y^s$ have $m_y > 0$.

Flux ratios

Apparent magnitudes provide a simple relationship in which the ratio of the band pass fluxes of two distinct objects can be determined by the difference of their apparent magnitudes. Through the definition of magnitudes (Eq. 5.37), we have

$$m_y^{(1)} - m_y^{(2)} = -2.5 \log \left\{ \frac{F_y^{(1)}}{F_y^s} \right\} + 2.5 \log \left\{ \frac{F_y^{(2)}}{F_y^s} \right\} = -2.5 \log \left\{ \frac{F_y^{(1)}}{F_y^{(2)}} \right\}, \quad (5.38)$$

which can be inverted to obtain,

$$\frac{F_y^{(1)}}{F_y^{(2)}} = 10^{-0.4\left[m_y^{(1)} - m_y^{(2)}\right]}. \quad (5.39)$$

Note that every integer difference in the magnitudes of two objects corresponds to a factor of $10^{-0.4} = 2.5$ in their flux ratios. The term "dex" is often used; it is shorthand for "decade" on the logarithmic scale. For instance, the flux ratio of ± 2.5 corresponds to ∓ 0.4 [dex] on the magnitude scale.

5.6.2 Photometric systems

There are two main photometric systems employed in the astronomical sciences, the Vega system and the AB system. There are a plethora of filter suites, including the Johnson–Cousins, Washington, Gunn, Sloan Digital Sky Survey, Hipparcos–Tycho, and *Hubble Space Telescope* WFPC–2 and 3, and ACIS sets. For a general review see Bessell (2005). For brevity, we employ the Johnson–Cousin $UBVRI$ system for purposes of illustration. The $UVBRI$ filter response functions (renormalized to a peak transmission of unity) are illustrated in Figure 5.7. For example, the $y = V$ ("visual" band) filter has an effective central wavelength of 5500 Å with a band pass ranging from 4700–7400 Å.

Vega system

The Vega system is calibrated using the flux density of the A0 V star Vega (or sometimes the mean of a sample of unreddenned A0 V Pop I stars). The flux density of Vega (Oke, 1990)[1] is presented in Figure 5.7 as the thin solid

[1]The electronic data were obtained from the on–line archive of optical and UV spectrophotmetric flux standard stars made available by the European Southern Observatory. (*http://www.eso.org/sci/observing/tools/standards/spectra/*)

curve (with absorption features). Because A0 V stars do not have a flat flux density, the calibration band pass flux, $F_y^{(\mathrm{Vega})}$ is different for each band pass. For additional information see Oke & Gunn (1983); Bessell (1990). For information on the Sloan filter suite and calibration, see Smith *et al.* (2002).

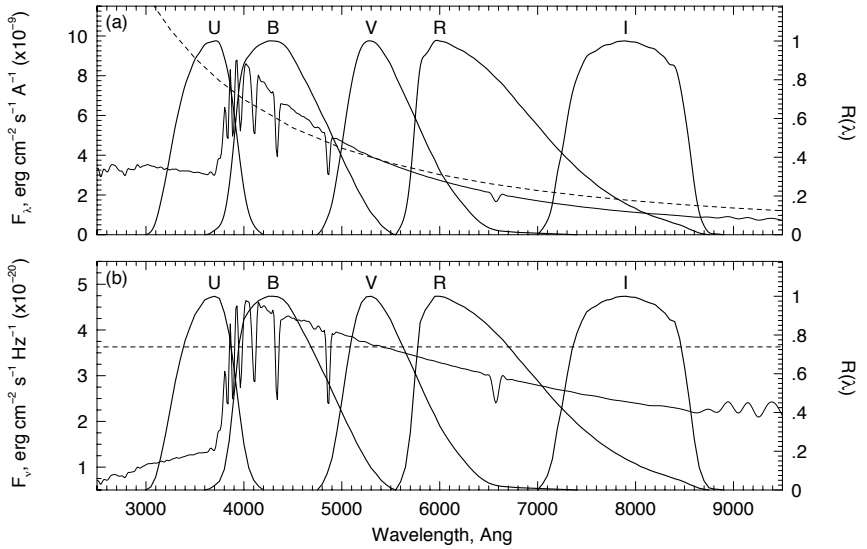

Figure 5.7: (*a*) The flux densities, F_λ, of Vega (thin solid curve) and the hypothetical AB source (dashed curve). (*b*) The flux densities, F_ν, of Vega (thin solid curve) and the hypothetical AB source (dashed curve). Superimposed are the Johnson–Cousins $UBVRI$ filter response curves normalized to unity at their peak transmissions. The differences between the calibration magnitude of Vega and that of the AB magnitude are listed in Table 5.1.

AB system

For AB magnitudes, there is no physical standard source, but simply a definition of a hypothetical source with $F_\nu^{(\mathrm{AB})} = 3.63 \times 10^{-20}$ [erg s^{-1} cm^{-2} Hz^{-1}] for all ν (a flat frequency flux density distribution). This is not a flat flux density in wavelength, $F_\lambda^{(\mathrm{AB})} = 0.1092/\lambda^2$ [erg s^{-1} cm^{-2} Å^{-1}] (where λ is [angströms]). The AB flux density is presented in Figure 5.7 as the thin dashed curve.

Because F_ν is a constant, and the filter responses have unity normalization (Eq. 5.35), we have $F_y^{(\mathrm{AB})} = F_\nu^{(\mathrm{AB})}$, yielding $-2.5\log\{3.63\times10^{-20}\} = 48.60$. Thus, from the definition of apparent magnitude (Eq. 5.37),

$$m_y(\mathrm{AB}) = -2.5\log F_y - 48.60 = -2.5\log F_\nu - 48.60 = m_\nu - 48.60 \qquad (5.40)$$

for all band passes, where m_ν is the magnitude of the flux density as defined in Eq. 5.36. Note that Eq. 5.40 (and the constant -48.60) applies only if the band pass flux is determined using frequency units. As such, AB magnitudes in frequncy units are equivalent to the flux density magnitude, m_ν, scaled to the hypothetical AB source.

Contrasting systems

In Figure 5.7*a*, the standard Vega and AB flux density distributions, $F_\lambda^{(\mathrm{Vega})}$ and $F_\lambda^{(\mathrm{AB})}$, are shown. In Figure 5.7*b*, $F_\nu^{(\mathrm{Vega})}$ and $F_\lambda^{(\mathrm{AB})}$ are shown. The Johnson–Cousins $UVBRI$ band pass response curves[2] are superimposed (thick solid curves). Vega is shown as the thin solid curve (which exhibits aborption features), and the AB source is shown as the smooth dashed curve. The definition of the AB standard "source" flux density was chosen to give $m_V(\mathrm{AB}) = m_V$, or more precisely

$$\int_{4700}^{7400} R_V(\lambda)\, F_\lambda^{(\mathrm{Vega})}\, d\lambda = \int_{4700}^{7400} R_V(\lambda)\, F_\lambda^{(\mathrm{AB})}\, d\lambda\,, \tag{5.41}$$

(or the equivalent integrals over frequency). However, the latest calibration of Vega yields a difference of 0.044 magnitudes. Note that the flux density curves are normalized (by definition for AB magnitudes) near the center of the response curve for the V filter.

In Table 5.1, the central (effective) wavelength, λ_y, and the band pass width, $\Delta\lambda_y/\lambda_y$, are listed for the Johnson–Cousins $UBVRI$ filter suite. Also listed are the values of $F_\nu^{(\mathrm{Vega})}$ [erg s^{-1} cm^{-2} Hz^{-1}] at ν_y and $F_\lambda^{(\mathrm{Vega})}$ [erg s^{-1} cm^{-2} Å^{-1}] at λ_y. The values of the latter can be visually confirmed by inspection of Figure 5.7. The last column lists the magnitude difference between the Johnson–Cousins Vega system and the Johnson–Cousins AB system, $m_y - m_y(\mathrm{AB}) = \Delta m_y$, i.e., the quantity added to the Johnson magnitude in band pass y to obtain the AB magnitude in that band pass.

Table 5.1: Vega and AB Magnitude Data

Band pass (y)	λ_y [Å]	$\Delta\lambda_y/\lambda_y$	$F_\nu^{(\mathrm{Vega})}$ [10^{-20}]	$F_\lambda^{(\mathrm{Vega})}$ [10^{-9}]	Δm_y
U	3600	0.15	1.81	3.18	$\cdots$
B	4400	0.22	4.26	6.60	-0.163
V	5500	0.16	3.64	3.61	-0.044
R	6400	0.23	3.08	2.26	$+0.055$
I	7900	0.19	2.55	1.23	$+0.309$

In imaging studies, one measures F_y directly. In spectroscopic studies, F_y must be computed using Eq. 5.34 from the measured F_λ or F_ν. In practice, imaging studies are almost always more accurate because accurately measuring the flux spectroscopically is complicated by additional wavelength effects. In particular, one must be sure that all the light from the object passes through

[2]Electronic data from *ftp://ftp.noao.edu/kpno/filters/4Inch_List.html* .

the slit (if the slit is narrower than the seeing disk of the object, then some light will be lost at the slit).

5.6.3 Absolute magnitude and luminosity

The absolute magnitude in band pass y, M_y, is defined as the apparent magnitude that an observer would measure at a distance of $D = 10$ [pc] from the source. Whereas apparent magnitude differences relate band pass flux ratios, absolute magnitude differences relate band pass luminosity ratios. Thus, in a sense, M_y is a surrogate for band–pass luminosity through the normalization of the band–pass flux to a standardized distance. To account for the finite band pass, the luminosity density, L_λ, is employed,

$$L(\lambda) = \lambda L_\lambda, \tag{5.42}$$

where $L(\lambda)$ is in [units erg s^{-1}], and L_λ is in units [erg s^{-1} Å^{-1}]. The coversion from L_λ to L_ν follows the relations for the flux density as given in Eq. 5.33. The integrated luminosity in the band pass is

$$L_y = \int_{\lambda_{y^-}}^{\lambda_{y^+}} R_y(\lambda) \lambda L_\lambda \, d\lambda \, . \tag{5.43}$$

The relationship between the flux density and the luminosity density is

$$F_\lambda = \frac{L_\lambda}{4\pi D^2}. \tag{5.44}$$

From Eqs. 5.34, 5.37 and 5.44, the apparent magnitude of an object observed in band pass y can be written in terms of luminosity

$$m_y = -2.5 \log \left\{ \int_{\lambda_{y^-}}^{\lambda_{y^+}} R_y(\lambda) \frac{\lambda L_\lambda}{4\pi D^2} \, d\lambda \right\} + 2.5 \log F_y^s. \tag{5.45}$$

By definition, the absolute magnitude is obtained by setting $D = 10$ [pc],

$$M_y = -2.5 \log \left\{ \int_{\lambda_{y^-}}^{\lambda_{y^+}} R_y(\lambda) \frac{\lambda L_\lambda}{4\pi (10 \text{ pc})^2} \, d\lambda \right\} + 2.5 \log F_y^s, \tag{5.46}$$

The difference of the above two equations, $m_y - M_y$, is called the distance modulus, denoted DM,

$$\text{DM} = 5 \log \left\{ \frac{D}{10 \text{ pc}} \right\} = 5 \log D - 5, \tag{5.47}$$

where the distance to the object, D, is expressed in [parsecs]. Thus, if the apparent magnitude and distance to an object is measured, the absolute magnitude can be computed from

$$M_y = m_y - \text{DM}, \tag{5.48}$$

Often, for a population of object (such as galaxies, etc.), there is a measured characteristic absolute magnitude, M_y^*, for the band pass, which, according to Eq. 5.46, corresponds to a characterstic luminosity for the band pass, L_y^*. This characteristic luminosity might be, for example, the average band pass luminosity for a population of object. Through the definition of magnitudes (Eqs. 5.37 and 5.46), and applying steps analagous to those obtained to derive Eq. 5.38, we have

$$M_y - M_y^* = -2.5 \log \left\{ \frac{L_y}{L_y^*} \right\}, \tag{5.49}$$

which can be inverted to obtain the ratio of the luminosity of the object to the characteristic luminosity of the population,

$$\frac{L_y}{L_y^*} = 10^{-0.4\left[M_y - M_y^*\right]}. \tag{5.50}$$

5.6.4 Cosmological Sources

The above treatment of the apparent and absolute magnitudes presupposes that the source object is in the same cosmological reference frame as the observer. Cosmological objects can have substantially redshifted spectral energy distributions, such that the flux density observed in band pass y at the observer does not correspond to the same band pass in the frame of the source. The cosmological effects altering the observed flux density of a redshifted source are discussed in Chapter 14. These effects require that a corrective term be applied to the band pass flux integrals in order to deduce the apparent and absolute magnitude in the rest frame of the object. These corrections, called K–corrections, are discussed in § 14.7.

5.7 Atmospheric attenuated flux

The quantity F_λ is the observed flux incident upon the upper atmosphere of Earth. Before this flux is recorded for subsequent analysis, the beam first suffers wavelength dependent attenuation while passing through the atmosphere. We quantify the atmospheric transmission at wavelength λ as $\epsilon_\lambda^{\rm A}$, which equals the ratio of the flux entering the telescope to the observed flux entering the upper atmosphere, F_λ. The form of $\epsilon_\lambda^{\rm A}$ can be complex and include atmospheric absorption lines and bands, which are commonly known as telluric features. Furthermore, the magnitude of $\epsilon_\lambda^{\rm A}$ is proportional to the path length through the atmosphere.

Defining atmospheric attenuated flux as $F_\lambda^{\rm A}$,

$$\epsilon_\lambda^{\rm A} = \frac{F_\lambda^{\rm A}}{F_\lambda} = \exp\{-\tau_\lambda^{\rm A}\}, \tag{5.51}$$

where $\tau_\lambda^{\rm A}$ is the optical depth of the atmosphere. The optical depth increases with the zenith angle, denoted z, which is the angle of the line of sight to the

source measured from the local zenith of the telescope. For a constant density plane parallel model of the atmosphere,

$$\tau_\lambda^{\rm A}(z) = \tau_\lambda^{\rm A}(0)\sec z, \tag{5.52}$$

where $\tau_\lambda^{\rm A}(0)$ is the atmospheric optical depth at the zenith ($z = 0$). A commonly used term to quantify the attentuation through the atmosphere is the "airmass", defined as the ratio of the optical depth toward the zenith to the optical depth at zenith angle z,

$$\text{airmass} = \frac{\tau_\lambda^{\rm A}(z)}{\tau_\lambda^{\rm A}(0)} = \sec z. \tag{5.53}$$

Note that the $\sec z$ dependence applies only under the assumption of a constant density plane parallel atmosphere; it applies well for small z. Higher accuracy approximations can be found in Kasten & Young (1989). Technically, airmass of unity is defined at sea level, but it is common that this normalization is not included in the definition so that airmass is measured with respect to the local elevation of the telescope facility. Thus, the zenith sightline is referred to as "unit airmass". In the most general form, we have

$$\epsilon_\lambda^{\rm A}(z) = \exp\{-\tau_\lambda^{\rm A}(z)\}\,. \tag{5.54}$$

Thus, the flux entering the telescope at angle z from the zenith, which we call the "attenuated flux", is then given by

$$\tilde{F}_\lambda^{\rm A} = \epsilon_\lambda^{\rm A}(z)\,F_\lambda = \epsilon_\lambda^{\rm A}(z)\frac{R^2}{D^2}\,\mathcal{F}_\lambda \exp\{-\tau_\lambda\} = \tilde{F}_\lambda^{\rm A_0}\exp\{-\tau_\lambda\}\,, \tag{5.55}$$

where τ_λ is the optical depth of an absorption feature in the observed flux spectrum and the "attenuated continuum flux" (the attenuated flux in the absence of an intervening absorbing cloud ($\tau_\lambda = 0$) is

$$\tilde{F}_\lambda^{\rm A_0} = \epsilon_\lambda^{\rm A}(z)\frac{R^2}{D^2}\mathcal{F}_\lambda = \epsilon_\lambda^{\rm A}(z)\frac{R^2}{D^2}\,\pi\,\mathcal{I}_\lambda. \tag{5.56}$$

As we will discuss in detail in Chapter 6, further modification to the final recorded flux occurs as the light interacts with the optical elements of the telescope and the spectrograph before the light beam impinges upon the recording apparatus, i.e., the detector. Fortunately, all these attenuations and modifications are multiplicative, so that one can recover the observed flux, F_λ, via a process known as flux calibration (see Chapter 7).

References

Bessell, M. S. 1990, UBVRI passbands, Pub. Astron. Soc. Pac., **102**, 1181

Bessell, M. S. 2005, Standard photometric systems, *Ann. Rev. Astron. & Astroph.*, **43**, 293

Gray, D. F. 1992, *The Observational and Analysis of Stellar Photospheres*, Cambridge University Press

Gunn, J. E., & Peterson, B. A. 1965, On the density of neutral hydrogen in intergalactic space, *Ap. J.*, **142**, 1633

Kasten, F., & Young A. T. 1989, Revised optical air mass tables and approximation formula, *Applied Optics*, **28**, issue 22, 4734

Lanzetta, K., & Bowen, D. V. 1992, The kinematics of intermeidate–redshift gaseous galaxy halos, *Ap. J.*, **391**, 48

Mihalas, D. 1978, *Stellar Atmospheres*, W. H. Freeman & Company

Oke, J. B., & Gunn, J. E. 1983, "Secondary Standard Stars for Absolute Spectrophotometry," *Ap. J.*, **266**, 713

Oke, J. B. 1990, Faint spectrophotometric standard stars, *A. J.*, **99**, 1621

Smith, J. A., *et al.* 2002, "The u'g'r'i'z' standard–star system," *A. J.*, **123**, 2121

Weisheit, J. C. 1978, On the use of line shapes in the analysis of QSO absorption spectra, *Ap. J.*, **219**, 829

Vilkoviskij, Y, & Irwin, M. J. 2002, The spectrum of BAL Q1303+308: intrinisc variability and line locking stability, *M.N.R.A.S.*, **321**, 1